Appl Phys B (2011) 103:819–824
DOI 10.1007/s00340-011-4540-1

Applied Physics B
Lasers and Optics

Limitations of an optically pumped rubidium laser imposed by atom recycle rate

W.S. Miller · C.V. Sulham · J.C. Holtgrave · G.P. Perram

Received: 14 December 2010 / Revised version: 28 February 2011

Abstract A rubidium laser pumped on the $5^2S_{1/2}$–$5^2P_{3/2}$ D_2 transition by a pulsed dye laser at pump intensities exceeding 3.5 MW/cm^2 (>1000 times threshold) has been demonstrated. Output energies as high as 12 μJ/pulse are limited by the rate for collision relaxation of the pumped $^2P_{3/2}$ state to the upper laser $^2P_{1/2}$ state. More than 250 photons are available for every rubidium atom in the pumped volume during each pulse. For modest alkali atom and ethane spin–orbit relaxer concentrations, the gain medium can only process about 50 photons/atom during the 2–8 ns pump pulse. At 110°C and 550 Torr of ethane, the system is bottlenecked in the $^2P_{3/2}$ state and all of the incident photons cannot be absorbed. The output energy is linearly dependent on pump pulse duration for a given pump energy. The highly saturated pump limit of the recently developed three-level model for diode pumped alkali lasers (DPALs) is developed. The system efficiency based on absorbed photons approaches 36% even for these extreme pump conditions.

1 Introduction

The diode pumped alkali laser (DPAL) is a three-level laser employing an alkali vapor as the gain medium [1]. Optical excitation on the D_2 transition occurs between the ground $^2S_{1/2}$ state and the excited $^2P_{3/2}$ state. A population inversion between the $^2P_{1/2}$ and ground states is achieved by rapid collisional relaxation. The system efficiently converts un-phased diode laser pump photons into a single coherent beam by cycling alkali atoms through the pump–relaxation–lasing transitions at rates exceeding 10^{10} cycles/s per atom. A buffer gas mixture at near atmospheric pressure is typically required to broaden the absorption line shape and induce the collisional relaxation.

The first DPAL demonstration used Rb vapor as the gain medium with helium and ethane to line broaden the absorption line shape and induce spin–orbit relaxation [1]. DPAL devices based on Rb have been demonstrated at 0.4 W with a slope efficiency of 69% and 17 W at 53% efficiency [2, 3]. Similarly, the Cs system has achieved 0.35 W at 81%, 10 W at 68% and 48 W (quasi-cw) with 52% efficiency [4–6]. Most recently, a rubidium laser pumped by a 1.28-kW diode stack with a 0.35-nm bandwidth has achieved 145-W average power [7]. These efficient laser demonstrations have stimulated a great deal of interest in the high power laser community and scaling to higher average (cw) power is being actively pursued. The system offers an electrically driven laser with excellent thermal management, lightweight packaging and high brightness for commercial and military applications. Pulsed excitations, with surrogate pump sources, offer the opportunity to explore performance at high peak intensities for low cost.

The performance of the DPAL system is optimized when the spin–orbit relaxation rate is much faster than the optical pumping rate. Under these conditions, a quasi-two-level model predicts performance primarily limited by the matching of the pump and laser cavity mode volumes and cavity transmission losses [8]. These conditions are readily achieved at pump intensities of a few kW/cm^2. Recently, linear scaling of a Rb laser to 32 times threshold has been demonstrated [9]. However, scaling to pump intensities of >100 kW/cm^2 is largely unexplored.

The present paper examines the effects of bottlenecking imposed by insufficient spin–orbit relaxation at pump inten-

W.S. Miller · C.V. Sulham · J.C. Holtgrave · G.P. Perram (✉)
Department of Engineering Physics, Air Force Institute of Technology, 2950 Hobson Way, Wright-Patterson Air Force Base, OH 45433-7765, USA
e-mail: glen.perram@afit.edu

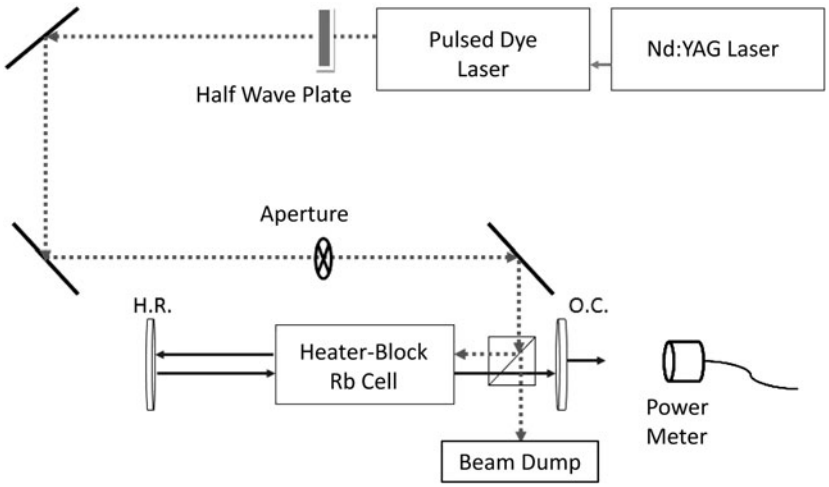

Fig. 1 Rb laser longitudinally pumped by a pulsed dye laser with variable pump pulse widths

sities exceeding 3.5 MW/cm^2 by employing a pulsed pump source. These conditions exceed pump threshold by more than a factor of 10^3. We also identify an analytic solution under the strongly saturated limit for the recently developed three-level DPAL model [8]. Alkali atoms are recycled many times during a single pulse, enabling a high ratio for the incident photons relative to the available atoms.

2 Experiment

The apparatus for the optically pumped rubidium laser is illustrated in Fig. 1. A frequency-doubled Quanta-Ray Pro Series pulsed Nd:YAG laser (10 Hz, 0–1 J/pulse, 532 nm) is used to pump a Sirah model PRSC-D-1800 dye laser with LDS-765 dye tuned to the Rb D_2 transition at 780.25 nm. The dye laser provides 2–8 ns pulses as the energy is tuned from 0 to 100 mJ/pulse by varying the Nd:YAG flashlamp energy. The dye laser output beam is limited by the iris and is relatively collimated with a 0.1-cm radius. The pump beam spot increases by about 18% as the pump energy increases by a factor of 2.5. The dye laser spectral width is ∼31 GHz and is ∼98% vertically polarized. At 0.5 mJ/pulse, the pump intensity is 2.2 MW/cm^2.

The Rb cell is 12.7-cm long × 2.5-cm diameter and includes a finger where the concentration of the alkali is controlled and a glass valve connected to the gas handling system. An aluminum heater block encloses the cell with a Watlow temperature controller connected to five cartridge heaters and a thermocouple on a negative-feedback loop to control the cell temperature. At 120°C the concentration of Rb inside the cell is 2.0×10^{13} cm^{-3}. The cell was filled at room temperature with ethane at 550 ± 10 Torr both to broaden the D_2 absorption line and to induce rapid relaxation between the two spin—orbit–split states, $^2P_{3/2,\,1/2}$. The Lorentzian (pressure broadened) FWHM line width at this pressure is 18 GHz [10]. A summary of pump laser and gain media parameters is provided in Table 1.

Table 1 Summary of laser parameters

Quantity	Variable	Nominal value
Pump energy	E_p	0.5 mJ
Pump duration	t_p	7.1 ns
Pump bandwidth	$\Delta\nu_p$	31 GHz
Pump volume	V_p	0.4 cm^3
Pump intensity	I_p	2.2 MW/cm^2
Rb concentration	n	2.0×10^{13} cm^{-3} at 120°C
Photons/atom	$(E_p/h\upsilon_p)/nV_p$	246
Cell temperature	T	383 K
Ethane concentration	$[C_2H_6]$	1.8×10^{19} cm^{-3}
Spin–orbit relaxation rate	k_{so}	4.7×10^{-10} cm^3/s
Number of cycles available	N_c	58
Absorption line width	$\Delta\nu_a$	18 GHz
Laser photon energy	$h\upsilon_l$	1.56 eV
Stimulated emission cross-section (D_1)	σ_{21} (ν_o)	3.23×10^{-13} cm^2
Saturation intensity (D_2)	I_{sat}	29.5 W/cm^2
Threshold gain	g_{th}	0.044 cm^{-1}
Threshold pump intensity	I_{th}	2.8 kW/cm^2
Threshold pump energy	E_{th}	0.64 μJ

The resonator is formed by a 50 cm radius of curvature maximum reflector and a flat 33% reflective output coupler separated by 42.5 cm. This stable resonator provides a Gaussian beam waist radius of 0.2 mm, which expands to about 0.55 mm at the curved mirror. The output beam spot size was not recorded, and the cavity mode volume may be underestimated. The pump beam is longitudinally coupled into the resonator via a polarizing beam splitter. The pump beam and output beams are counter-propagating. However,

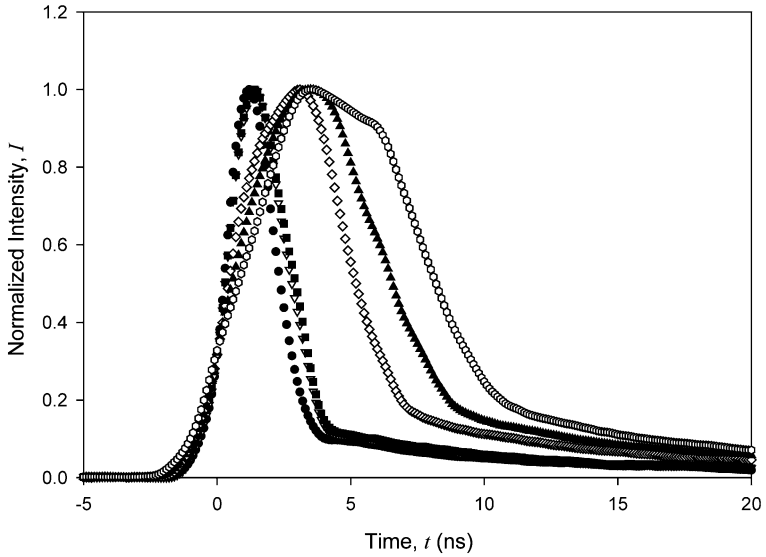

Fig. 2 Dye laser pulse shapes with widths (FWHM) of (●) 2.1 ns, (▽) 2.5 ns, (■) 2.6 ns, (◇) 5.1 ns, (◆) 5.4 ns and (○) 7.1 ns

little of the pump beam is absorbed and is reflected for a second pass through the gain medium.

The polarizing beam splitter and half-wave plate work in conjunction to control the pump energy delivered to the cell. Only the vertical polarization of the incoming beam is reflected into the cell with the remainder sent into a beam dump. By rotating the wave plate, the polarization of the incoming pump beam changes and a smaller percentage of the overall power is delivered to the alkali cell. A constant pump energy can be delivered to the cell by simultaneously varying both the wave plate and the Nd:YAG flashlamp energy. As the Nd:YAG energy increases, the pulse duration also increases from 2 to 8 ns. This approach allows for a study of the effects of pulse duration on the alkali laser output power for constant pump energy. While the pump beam quality is poor (multi-mode, elliptical spot) and degrades somewhat at lower pump energy, the pumped volume is primarily controlled by the iris. The influence of pump beam quality on DPAL performance has recently been characterized for a longer pulse, quasi-cw system [11] and was not investigated in the current work.

A New Focus fast photodetector was coupled to a Wavepro 7100 1-GHz oscilloscope to determine the pump and lasing pulse shapes. Several example pulse shapes are provided in Fig. 2. Average alkali laser power was measured with a Thorlabs S122B germanium detector incorporating an 800 nm (10 nm FWHM) band-pass filter providing sensitivity from 35 nW to 35 mW (3.5 nJ/pulse to 3.5 mJ/pulse).

3 Results

Figure 3 illustrates the rubidium laser energy for constant delivered pump energy as a function of wave-plate angle. A dramatic increase in the output energy is achieved when

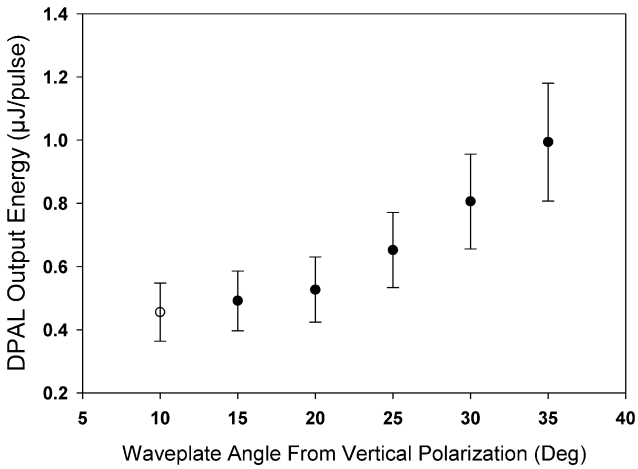

Fig. 3 Rb laser output energy for a fixed delivered pump energy of 4.5 mJ/pulse achieved by simultaneously varying the Nd:YAG energy/pulse and rotating the wave plate. The data points correspond approximately to the pulse shapes reported in Fig. 2

the wave plate induces a polarization that is largely crossed with the beam splitter so that a large fraction of the pump energy is dumped. Under these conditions, the dye laser pulse energy at the source is higher and the pulse duration is longer. This allows more time for alkali atom recycling as discussed below.

The rubidium laser output energy as a function of pump energy is shown in Fig. 4. The threshold as computed from the recently reported DPAL model [8] for the conditions of Table 1 is 0.64 μJ/pulse. All of the conditions presented in Fig. 4 represent highly bleached alkali samples. Indeed, all prior DPAL and surrogate DPAL demonstrations have been limited to pump conditions of less than 32 times threshold, whereas the lowest pump energy in the present work is ∼52 times threshold. The dye laser output energy is highly vari-

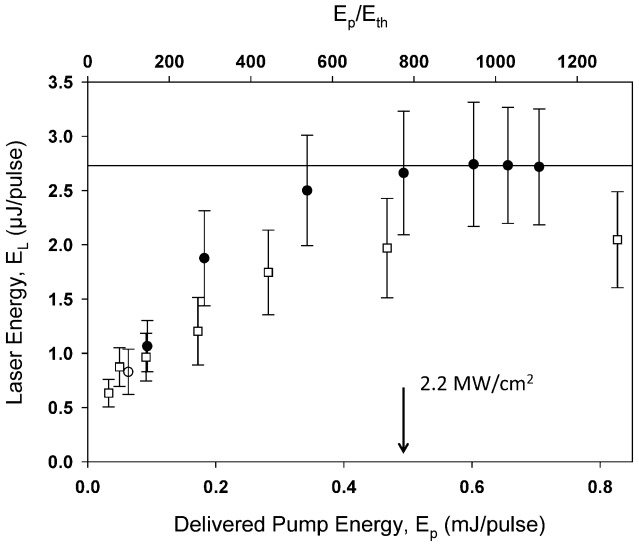

Fig. 4 Rb laser output energy as a function of delivered pulsed dye laser energy for pulse widths of (□) 2 ns and (●) 2.8 ns. The output energy is asymptotically limited under high pump intensity conditions

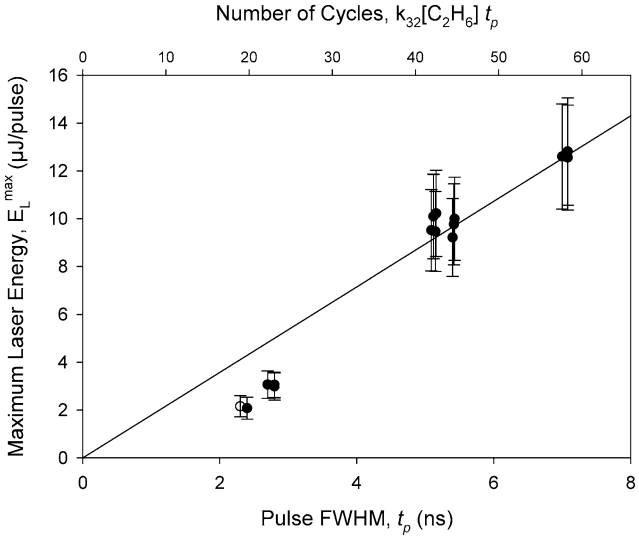

Fig. 5 Linear relationship between limiting output energy and pump pulse duration. The pump energy where the output energy is maximized increases from 0.5 mJ/pulse for the 2.3-ns pulse to 1.8 mJ/pulse for the 7.1-ns pulse

able from shot-to-shot at energies <20 μJ/pulse and a reliable observation of threshold is not obtainable.

The efficiencies based on incident pump energies from Fig. 4 are less than 1%, very low considering that most DPAL demonstrations achieve slope efficiencies of 30–80% [2–6]. For a pump energy of 0.5 mJ/pulse the pump intensity is 2.2 MW/cm^2 and there are 246 photons for every alkali atom in the pumped volume (see Table 1). Despite rapid recycling of the rubidium atoms as discussed below, the gain medium is unable to absorb all the pump energy during the short pump pulse duration.

An asymptotic limit to the output energy is reached as input energy is increased to >0.5 mJ/pulse. The output energy attained at this asymptotic limit depends upon pulse duration and is identified in Fig. 4 as 2.0 and 2.7 μJ/pulse for pulse durations of 2.3 and 2.8 ns, respectively. Data similar to those reported in Fig. 4 for pulse durations of 5.1, 5.4 and 7.1 ns were obtained and the resulting asymptotic output energies scale to greater than 13 μJ/pulse as reported in Fig. 5.

The interpretation of these results is aided by examining the three-level model for DPAL performance [8] in this high pump intensity limit. The populations of the ground $^2S_{1/2}$ state, n_1, pumped $^2P_{3/2}$ state, n_3, and upper laser $^2P_{1/2}$ state, n_2, are longitudinally averaged and assumed constant radially. The output Rb laser intensity, I_L, is related to the longitudinally averaged intra-cavity laser intensity, Ψ via output coupler reflectivity, r, and cavity and transmission losses, t:

$$I_L = \frac{\Psi[I_{Pin}]g_{th}l_g e^{g_{th}l_g}t(1-r)}{(e^{g_{th}l_g}-1)(1+t^2re^{g_{th}l_g})}, \tag{1}$$

where the threshold gain is defined as

$$g_{th} = -\frac{\ln(rt^4)}{2l_g} \tag{2}$$

and the gain length is $l_g = 12.7$ cm. For no cavity transmission losses, $t = 1$, the result is simply

$$I_L = \Psi[I_{Pin}]g_{th}l_g. \tag{3}$$

The dependence of the intra-cavity intensity on input intensity is provided by the key model result:

$$\Psi = \eta_o I_{sat}\left(\alpha\frac{2I_{Pin}}{I_{sat}} - \beta\right), \tag{4}$$

where

$$\alpha \equiv \frac{(\frac{\sigma_{21}n}{g_{th}})(2\kappa(1-e^{-\theta})(\frac{\Gamma_{31}}{\Gamma_{21}})-1)-(3+2(1+3e^{-\theta})\kappa(\frac{\Gamma_{31}}{\Gamma_{21}}))}{2[(1+\kappa(1+e^{-\theta}))+2\frac{2I_{Pin}}{I_{sat}}]}, \tag{5}$$

$$\beta \equiv \left(1+\frac{\sigma_{21}n}{g_{th}}\right)\left[\frac{1+\kappa(1+2(\frac{\Gamma_{31}}{\Gamma_{21}})e^{-\theta})}{2[(1+\kappa(1+e^{-\theta}))+2\frac{2I_{Pin}}{I_{sat}}]}\right]. \tag{6}$$

Here

κ = spin–orbit relaxation rate relative to the spontaneous rate = $k_{so}[C_2H_6]/\Gamma_{31} = 221.6$,

θ = spin–orbit splitting = $\Delta E/k_bT = 0.89$ (at T = 110°C),

Γ_{31}, Γ_{21} = radiative rates for D_2 and D_1 lines, respectively = 1/26.2 ns and 1/27.7 ns,

n = rubidum concentration = 2×10^{13} atoms/cm^3 at 120°C,
$\sigma_{21}(\nu_o)$ = homogeneously broadened stimulated emission cross-section at line center of the lasing transition = 3.23×10^{-13} cm^2,
$I_{sat} = (h\nu_p/\sigma_{31})\Gamma_{31} = 29.5$ W/cm^2.

For very highly bleached conditions (no significant pump intensity attenuation) with the pump beam reflected from the mirror for a second pass, the longitudinally averaged, intracavity pump intensity, Ω, is simply twice the incident pump intensity, $\Omega = 2I_{Pin}$. This condition has been utilized in (4)–(6). When the incident intensity is very high, $I_{Pin}/I_{sat} \gg \kappa$, the system is bottlenecked on the spin–orbit relaxation and

$$\lim_{I_{Pin}\to\infty} \alpha\left(\frac{2I_{Pin}}{I_{sat}}\right) = \frac{(\frac{\sigma_{21}n}{g_{th}})(2\kappa(1-e^{-\theta})(\frac{\Gamma_{31}}{\Gamma_{21}})-1)-(3+2(1+3e^{-\theta})\kappa(\frac{\Gamma_{31}}{\Gamma_{21}}))}{4}, \tag{7}$$

$$\lim_{I_{Pin}\to\infty} \beta = 0. \tag{8}$$

Furthermore, when the gain is large relative to threshold, $\sigma_{21}n/g_{th} \gg 1$, and the spin–orbit relaxation is reasonably fast, $\kappa \gg 1$, then the output intensity is linear dependent on alkali and buffer gas concentrations:

$$\lim_{I_{Pin}\to\infty} I_L \equiv I_L^{\infty} = \eta(h\nu_p)\,(nk_{32}M)\left(\frac{1-e^{-\theta}}{2}\right) \times \left(\frac{\Gamma_{31}}{\Gamma_{21}}\right)\left(\frac{\sigma_{21}}{\sigma_{31}}\right) l_g. \tag{9}$$

The concentration of ethane in the system, M, defines the spin–orbit mixing time. The slope efficiency, η, includes both the quantum efficiency, $\eta_o = (h\upsilon_L/h\upsilon_P)$, and the mode overlap, η_{mode}, for the pump beam (spatial distribution of the gain) and the spatial laser mode intensity distribution, I_{res}, associated with the cavity [8, 13]:

$$\eta_{mode} = \frac{\int \sigma_{21}[n_2(x,y,z) - n_1(x,y,z)]I_{res}(x,y,z)\,dx\,dy\,dz}{\int I_{res}^2(x,y,z)\,dx\,dy\,dz}. \tag{10}$$

Finally, the output energy per pulse is predicted as

$$E_L = I_L A t_p = \eta_{mode}(h\nu_L)(nV_p)(k_{32}Mt_p)\left(\frac{1-e^{-\theta}}{2}\right)\left(\frac{\Gamma_{31}}{\Gamma_{21}}\right)\left(\frac{\sigma_{21}}{\sigma_{31}}\right). \tag{11}$$

The final two factors reflect the difference in saturation intensity between the pump and lasing transitions, and it is nearly unity. Note that as the spin–orbit splitting becomes small, $\theta \to 0$, the output energy in the highly saturated limit approaches zero. That is, the system is approaching a two-level optically pumped laser, which cannot exhibit net gain. The number of atoms cycled through the spin–orbit relaxation process during the pulse duration is

$$N_c = k_{32}Mt_p. \tag{12}$$

Thus, the output energy is simply the product of the energy per photon, the number of alkali atoms participating in the inversion cycling and within the pumped volume, and the number of cycles per atom, modified by any mode overlap inefficiencies.

The increased output energy as the pulse duration increases for a fixed pump energy observed in Fig. 5 is consistent with the prediction of (10). The asymptotic limit is achieved at >0.5 mJ/pulse, or 2×10^{15} photons, for all the present conditions. There are 8×10^{12} Rb atoms in the 0.4 cm^3 pump volume, yielding >250 photons per atom. All these photons can be utilized only if the recycling rate is sufficiently high. The spin–orbit relaxation rate cross-section for ethane is 7.7×10^{-15} cm^2 [12]. At 550 Torr of ethane, this corresponds to a relaxation time of 0.12 ns. Assuming that the spin–orbit relaxation is rate limiting, there is time for only 58 cycles during the longest of the pump pulses. As the pulse duration is shortened to 2 ns at the same energy, even fewer cycles are available, less of the pump beam is absorbed and the laser output energy is further reduced. The system is bottlenecked by the spin–orbit relaxation process. To increase output energy, either the cell temperature should be increased to enable higher alkali vapor pressures, or the ethane pressure increased. These conditions imply higher reactivity of the ethane where soot deposits and light-induced precipitates have been observed. High-pressure heat pipes and alternative species for spin–orbit relaxation may be required to achieve these conditions.

The predicted output energy for a mode overlap efficiency of $\eta_{mode} = 0.36$ is overlaid with the experimental results in Fig. 5. The Gaussian TEM$_{oo}$ cavity mode volume relative to the observed pump spot size–gain length product is $V_c/V_p = 0.12$. However, the output laser spot size was not determined in the present apparatus, and most DPAL demonstrations achieve mode overlaps (slope efficiencies) of 0.3–0.8 [2–7]. Multi-transverse mode operation is giving the poor beam quality of the pump source. The shortest pump pulses perform somewhat poorer than predicted, presumably due to photon buildup times and temporal dynamics associated with threshold. Indeed, the cavity round trip time is 2.8 ns, longer than the shortest pump pulse.

4 Conclusions

A rubidium DPAL type laser using a pulsed surrogate pump source has been demonstrated at pump intensities exceeding 10^3 times threshold, 30 times greater than previously achieved. The output intensity scales approximately linearly with pump pulse duration even with the pump intensity is constant. Remarkably, each alkali atom cannot be cycled more than 50 times during a 7.1-ns pulse, or at rates of $>10^{10}$ photons/atom/s, limited by the spin–orbit relaxation rate. Even at pump intensities exceeding 4 MW/cm^2, the absorbed photon system efficiency is greater than 30%, and likely limited by mode overlap. The identification of a new limiting case for the recently published level DPAL model provides an acceptable interpretation of the data. No evidence for energy pooling, ionization or nonlinear processes that dramatically degrade system performance was observed. Improved output energy could be achieved by increasing either alkali or spin–orbit relaxer concentrations.

Acknowledgements This work was supported by a grant from the High Energy Laser Joint Technology Office and the Air Force Office of Scientific Research.

References

1. W.F. Krupke, R.J. Beach, V.K. Kanz, S.A. Payne, Opt. Lett. **28**, 2336 (2003)
2. T.A. Perschbacher, D.A. Hostutler, T.M. Shay, in *XVI Int. Symp. Gas Flow and Chemical Lasers and High Power Laser Conf.*, Gmunden, Austria (2006)
3. B.V. Zhdanov, A. Stooke, G. Boyadjian, A. Voci, R.J. Knize, Opt. Lett. **33**, 414 (2008)
4. B.V. Zhdanov, T. Ehrenreich, R.J. Knize, Opt. Commun. **260**, 696 (2006)
5. B. Zhdanov, R.J. Knize, Opt. Lett. **15**, 2167 (2007)
6. B.V. Zhdanov, J. Sell, R.J. Knize, Electron. Lett. **44**, 582 (2008)
7. J. Zweiback, B. Krupke, Proc. SPIE **7581**, 75810G (2010)
8. G.D. Hager, G.P. Perram, Appl. Phys. B **101**, 45 (2010)
9. C.S. Sulham, G.P. Perram, M.P. Wilkinson, D.A. Hostutler, Opt. Commun. **283**, 4328 (2010)
10. N.D. Zameroski, G.D. Hager, W. Rudolph, C.J. Erickson, D.A. Hostutler, J. Quant. Spectrosc. Radiat. Transf. **112**, 59 (2011)
11. N.D. Zameroski, G.D. Hager, W. Rudolph, D.A. Hostutler, J. Opt. Soc. Am. B (2011, accepted)
12. E.S. Hrycyshyn, L. Krause, Can. J. Phys. **48**, 2761 (1970)
13. T.Y. Fan, R.L. Byer, IEEE J. Quantum Electron. **QE-23**, 605 (1987)